Continuum-plasma solution surrounding nonemitting spherical bodies

Continuum-plasma solution surrounding non-emitting spherical bodies

Leonardo Patacchini and Ian H. Hutchinson

Plasma Science and Fusion Center and

Department of Nuclear Science and Engineering

Massachusetts Institute of Technology

Cambridge, MA 02139, USA.

email: patacchi@psfc.mit.edu

Abstract

The classical problem of the interaction of a non-emitting spherical body with a zero mean-free-path continuum plasma is solved numerically in the full range of physically allowed free parameters (electron Debye length to body radius ratio, ion to electron temperature ratio, and body bias), and analytically in rigorously defined asymptotic regimes (weak and strong bias, weak and strong shielding, thin and thick sheath). Results include current-voltage characteristics as well as floating potential and capacitance, for both continuum and collisionless electrons. Our numerical computations show that for most combinations of physical parameters, there exists a closest asymptotic regime whose analytic solutions are accurate to 15% or better.

1 Introduction

1.1 Background

Theoretical analysis of flux-sensing probes' [1] operation in stationary, weakly ionized plasmas where the ion and electron mean-free-paths $L_{i,e}$ are much shorter than the probe dimensions and the electron Debye length Λ_{De} (continuum regime) has a long history. Indeed by assuming that ion and electron transport reduces to the mobility-diffusion equations

$$\mathbf{\Gamma_{i,e}} = -D_{i,e}\nabla N_{i,e} - \mu_{i,e} N_{i,e} \nabla V, \tag{1}$$

approximate analytic or reasonably simple numerical treatments yielding current-voltage characteristics become possible for probes with spherical geometry. In Eq. (1) $\Gamma_{i,e}$, $N_{i,e}$, $D_{i,e}$ and $\mu_{i,e}$ are respectively the ion (electron) flux density, density, diffusivity and mobility; V is the self-consistent electrostatic potential governed by Poisson's equation

$$\nabla^2 V = \frac{1}{\epsilon_0}(N_e - N_i). \tag{2}$$

Most of the interesting theoretical work on this model was done in the years 1960s/70s, and the relevant literature up to 1975 usefully reviewed in Refs [2, 3].

Interestingly enough, little application for those theories existed in their early days, and in fact ad hoc experiments were built for the sole purpose of verifying their validity [4, 5]. With the recent development of plasma-processing technologies however, probe diagnostics are today widely used in high pressure discharges where continuum conditions are easily satisfied; this naturally calls for further development of the yet incomplete theory of continuum probes.

Also recent is the interest for Dusty plasmas [6], containing micrometer-size particles the charging of which shares many properties with the just-discussed probes. Although dust grains are typically two to four orders of magnitude smaller than probes ($\sim 1 - 100\mu m$ for the former versus $\sim 1 - 10mm$ for the latter), experiments at nearly atmospheric pressure where the continuum theory of current collection can be applied have been conducted [7].

A fundamental difference between probes and dust particles is that probes are biased by an external circuit, while dust particles must float to balance ion and electron fluxes. Because of the high electron to ion mobility ratio, the floating potential of a non-emitting body is negative, as are the typical operating points of a probe.

1.2 Previous approaches to the "probe" problem

In their classical paper [8], Su and Lam cast the mobility-diffusion equations for ion and electron transport to a spherical probe of radius R_p and negative potential V_p (1) as an initial value problem by neglecting the high order non-linearities and limiting themselves to $\Lambda_{De} \lesssim R_p$, where by " $\lesssim$ " we mean less or approximately equal. Both an approximate analytic treatment for weak probe biases and numerical for strong biases was proposed. In this particular case, strong bias entails $|V_p| \gg T_{i,e}/e$, where $T_{i,e}$ is the ion (electron) temperature of the unperturbed plasma. For our purposes, the most valuable part of Su and Lam's paper is the theoretical analysis of the continuum model rather than its numerical solution. In fact a significant part of today's available literature on the subject "rediscovers" ideas already present, although not obviously, in Ref. [8].

Simultaneously, Cohen [9] completed Su and Lam's results with a numerical treatment in the moderate bias regime ($|V_p| \lesssim 10T_e/e$), still assuming $\Lambda_{De} \lesssim R_p$.

Su and Lam's, as well as Cohen's results have been commented on by Baum and Chapkis [10], who published numerical solutions in the entire range $0 < \Lambda_{De}/R_p < \infty$ when $T_i = T_e$. Unfortunately they limit themselves to moderate potentials, and so did the authors of Refs [11, 12, 5] ($|V_p| \lesssim 500T_e/e$), leading to confusing conclusions concerning asymptotic properties of the current-voltage characteristics. Furthermore, to our knowledge no complete results in the regime of cold ions ($T_i < T_e$) are available.

The previously cited treatments solve the simplest possible self-consistent formulation of the continuum probe problem. In particular the body is assumed to be thermalized with the background gas, and non-emitting. Relaxation of the first hypothesis has been discussed by Thomas [13] and by Chapkis and Baum [14]; while the effect of electron emission (photoemission, secondary emission, or thermionic emission) has recently received interest in the context of dusty plasmas [15]. Ionization or recombination will be neglected as well. A further point to keep in mind is that in those same treatments the transport coefficients D and μ are uniform and related by Einstein's formula ($D_i = T_i\mu_i/m_i$ and $D_e = -T_e\mu_e/m_e$). Those assumptions are not valid when probe-induced electric fields are too strong [16], i.e. $|\mu_{i,e}\nabla V| \gtrsim \sqrt{T_{i,e}/m_{i,e}}$; in this case a full kinetic treatment, such as Ref. [17], might be more appropriate. Further development on those effects is out of the scope of the present publication.

1.3 Previous approaches to the "dust" problem

Many treatments specific to dust particles focus on the large Debye length or "Coulomb" regime, loosely corresponding to $\Lambda_{De} \gg \max(R_p, -eV_p/T_i, -eV_p/T_e)$ (a more rigorous definition will be proposed). This allows to calculate the ion and electron fluxes analytically with the assumption that the potential distribution is $V(R) = V_p R_p/R$ [14] , and from there obtain a first order correction to the plasma profiles (directly as in the appendix of Ref. [8], or after Fourier analysis of the governing equations as in Ref. [18]).

We have so far considered both the ion and electron species to be in the continuum regime. When treating micrometer-size dust particles in noble gases however, an interesting regime to analyze is when the ion transport obeys Eq. (1) but the electrons are collisionless: a Kinetic Electrons plasma (KE), as opposed to a Continuum Electrons plasma (CE). To our knowledge little specific work on the KE regime is available, and the reader is referred to Ref. [19] for some preliminary considerations.

For probes with strong negative bias the electrons can be shown to be Boltzmann distributed ($N_e = N_\infty \exp(eV/T_e)$) down to a "thin" layer at the collector's surface, where their density is negligible. This is valid in both KE [1] and CE [8] plasmas. Profiles (hence ion flux) in KE and CE plasmas are therefore only distinguishable for weak enough probe biases.

In this publication, we will refer to the term "probe" regardless of the physical nature of the collector.

1.4 Structure of this publication

The purpose of this publication is twofold. First we find the current-voltage characteristics, floating potential and capacitance of a spherical probe in CE and KE plasmas, in the range $0 < \Lambda_{De}/R_p < \infty$ and $0 > V_p > -10^5 T_i/e$. To do so we solve the coupled set of mobility-diffusion and Poisson's equations (1,2), using a Finite Element Method with linear basis functions for the potential and exponential basis functions for the ion and electron densities. We consider $0.01T_e \leq T_i \leq T_e$ for

KE plasmas, but limit ourselves to $0.1T_e \leq T_i \leq T_e$ for CE plasmas, since continuum electrons can hardly sustain a strong temperature difference with the background neutrals.

Second we build on the major available analytic treatments of the continuum problem, mostly from Ref. [8], to derive analytic solutions in a set of well defined asymptotic regimes (Weak/moderate and strong bias, weak shielding and Coulomb regime, thin and thick sheath). Those solutions, conveniently referenced in Tab. 2, facilitate the interpretation of our numerical computations. They should however be considered as valuable results per se, as we show that for most combinations of physical parameters, there exists a closest asymptotic regime whose analytic solutions are accurate to 15% or better.

2 Statement of the continuum problem

2.1 Continuum model

We study a neutral, weakly ionized plasma of singly charged ions and electrons with density at infinity $N_i = N_e = N_\infty$, perturbed by a spherical probe of radius R_p placed at the origin. The charged particles' density is much smaller than the neutrals' $(N_e, N_i \ll N_n)$; consequently only ion-neutral and electron-neutral collisionality effects are considered. Ionization and recombination are neglected in the probe vicinity, hence ion and electron flux-densities $\mathbf{\Gamma_{i,e}}$ are conserved.

Two different plasma models are considered, describing two possible opposite collisional behaviours of the electrons.

2.1.1 Continuum Electrons (CE)

In Continuum Electrons (CE) plasmas, both the ions and electrons are strongly collisional, and $\mathbf{\Gamma_{i,e}}$ obey mobility-diffusion equations (1) with uniform mobility and diffusion coefficients $\mu_{i,e}$ and $D_{i,e}$. Those are closed by flux conservation ($\nabla \mathbf{\Gamma_{i,e}} = 0$), and coupled through Poisson's equation (2).

We define the normalized potential $\phi = eV/T_e$, ion temperature $\tau = T_i/T_e$, densities $n_{i,e} = N_{i,e}/N_\infty$ and electron Debye length $\lambda_{De} = \Lambda_{De}/R_p$ ($\Lambda_{De} = \sqrt{\epsilon_0 T_e/N_\infty e^2}$). Capital letters refer to dimensional quantities while low-case characters refer to their dimensionless counterpart. All lengths are normalized to the probe radius R_p, hence $r_p = 1$.

If we further assume that the mobility and diffusion coefficients obey Einstein's relation $D_{i,e} = \pm T_{i,e}\mu_{i,e}/e$, our one-dimensional problem can be reduced to:

$$\begin{cases} \nabla\left(-\frac{\partial n_i}{\partial r} - \frac{1}{\tau} n_i \frac{\partial \phi}{\partial r}\right) & = & 0 \\ \nabla\left(-\frac{\partial n_e}{\partial r} + n_e \frac{\partial \phi}{\partial r}\right) & = & 0 \\ \nabla\left(\frac{\partial \phi}{\partial r}\right) - \frac{1}{\lambda_{De}^2}(n_e - n_i) & = & 0, \end{cases} \tag{3}$$

where the divergence operator is $\nabla(x) = 1/r^2\partial/\partial r(r^2 x)$. The potential boundary conditions are $\phi(r_p) = \phi_p$ (probe potential) and $\phi(\infty) = 0$. When the ion and electron mean-free-paths are much shorter than the probe radius, we can use as density boundary conditions $n_{i,e}(r_p) = 0$ and $n_{i,e}(\infty) = 1$ [3, 20].

After solving Sys. (3) with the above boundary conditions, the dimensional ion flux density to the probe is given by

$$\Gamma_i^p = \frac{N_\infty D_i}{R_p} \frac{\partial n_i}{\partial r}(r_p). \tag{4}$$

In Eq. (4) no role is played by the potential gradient at the probe surface since the density there is zero. Similarly, the electron flux density is $\Gamma_e^p = (N_\infty D_e/R_p)\partial n_e/\partial r(r_p)$. The "+" signs in front of the density gradients are chosen to have a positive flux in the probe direction (decreasing r).

The total ion (electron) current is then given by

$$I_{i,e} = 4\pi R_p^2 \Gamma_{i,e}^p. \tag{5}$$

2.1.2 Kinetic Electrons (KE)

In nobles gases, ions suffer resonant charge exchange collisions, and it is not uncommon for their mean-free-path to be much shorter than the electron's. It is therefore of interest to consider Kinetic Electrons (KE) plasmas, where electrons are assumed collisionless.

If there is no potential well around the negatively charged sphere (in particular no potential minimum below ϕ_p), the electron density only depends on the local potential and position (see for instance Eq. (8.41) in Ref. [21]):

$$n_e(\phi, r) = \frac{1}{2}e^{\phi}\left\{1 + \text{ erf }\left(\sqrt{\phi - \phi_p}\right) + \frac{\sqrt{r^2-1}}{r}\exp\left(\frac{\phi-\phi_p}{r^2-1}\right)\left[1 - \text{ erf }\left(r\sqrt{\frac{\phi-\phi_p}{r^2-1}}\right)\right]\right\}; \quad (6)$$

the problem therefore amounts to solving

$$\begin{cases} \nabla\left(-\frac{\partial n_i}{\partial r} - \frac{1}{\tau}n_i\frac{\partial \phi}{\partial r}\right) & = & 0 \\ \nabla\left(\frac{\partial \phi}{\partial r}\right) - \frac{1}{\lambda_{De}^2}(n_e(\phi, r) - n_i) & = & 0. \end{cases} \quad (7)$$

The electron flux density is in this case thermal

$$\Gamma_e^p = \frac{N_\infty D_e^{\text{app}}}{R_p}e^{\phi_p} = \Gamma_e^0 e^{\phi_p}, \quad (8)$$

where D_e^{app} is an apparent diffusion coefficient given by

$$D_e^{\text{app}} = R_p\frac{v_{te}}{2\sqrt{\pi}}. \quad (9)$$

Here $v_{te} = \sqrt{2T_e/m_e}$ is the electron thermal speed.

If $0 \geq \phi \gg \phi_p$ and/or $r \gg 1$, Eq. (6) reduces to

$$n_e(\phi, r) = e^{\phi}, \quad (10)$$

hence the electrons are Boltzmann distributed. It is common approximation to use Eq. (10) instead of Eq. (6), but as we will see our numerical procedure allows to account for the exact electron density distribution at little cost.

If the potential distribution has a minimum below ϕ_p, Eq. (6) is not valid and the electron density depends on the full potential profile. It is not possible in that case to devise formulas such as Eqs (6,8), and the electron Vlasov equation must be solved (via a Particle In Cell code for instance), which is out of the scope of this publication. Because it is not possible to know before solving Sys. (7) if the potential dips below ϕ_p or not, we need to extend Eq. (6) in order to handle such situations. We use:

$$n_e^{\text{ext}}(\phi, r) = \begin{cases} n_e(\phi, \frac{r}{r_{\min}}) & r > r_{\min} \\ \frac{1}{2}\exp(\phi_{\min}) & r \leq r_{\min}, \end{cases} \tag{11}$$

where $\phi_{\min}$ is the minimum value of the potential (maximum of $|\phi|$) reached at $r_{\min}$. When we compute the probe floating potential, the electron flux is required and we replace $\exp(\phi_p)$ by $\exp(\phi_{\min})r_{\min}^2$ in Eq. (8). Of course Eq. (11) and the fixing on Eq. (8) are at most heuristic recipes, required to avoid singularities in the code operation, and we do not claim any precision on their validity. As we will see, weakly biased probes in KE plasmas indeed produce non monotonic potential profiles.

Both the CE and KE models depend on the three dimensionless parameters λ_{De}, τ, and ϕ_p. The diffusion coefficients D_i, D_e or D_e^{app} are only required a posteriori, to calculate dimensional flux densities and floating potentials.

2.2 Solution method

Solving Sys. (3) or Sys. (7) presents three main difficulties. (a) The equations are coupled, (b) non linear, and (c) the mobility-diffusion equation for the attracted species (the ions) is highly hyperbolic when $|\phi_p|/\tau \gg 1$ and/or $\lambda_{De} \ll 1$.

Our approach to solving the problem is to use the Lagrangian Finite Element Method (FEM), that we here detail for KE plasmas. Application to CE plasmas is then straightforward.

2.2.1 Finite Element discretization

We consider a (N+1)-points grid r^j ($j \in [0 : N]$) defining N elements $K^j = [r^{j-1} : r^j]$ ($j \in [1 : N]$). We associate a set of basis functions Ψ^j to each node, such that $\Psi^j(r^j) = 1$ and $\Psi^j(r^{j\pm1}) = 0$. The numerical approximations of the unknowns n_i and ϕ then take the form:

$$n_i(r) = \sum_{j=0}^{N} n_i^j \Psi_i^j(r) \tag{12}$$

$$\phi(r) = \sum_{j=0}^{N} \phi^j \Psi_\phi^j(r). \tag{13}$$

The unknowns are n_i^j and ϕ^j, values of the approximated solutions at the node points. Because Sys. (7) is coupled, we simultaneously solve for the vector $u^j = (n_i^j; \phi^j)$ ($j \in [0 : N]$), but the basis functions Ψ_i^j and Ψ_ϕ^j need not be the same.

We use simple linear basis functions for the potential ϕ:

$$\Psi_\phi^j(\xi) = \begin{cases} 1-\xi & \xi \in [0;1] \\ 1+\xi & \xi \in [-1;0] \\ 0 & \text{otherwise,} \end{cases} \tag{14}$$

with mapping

$$\xi = \begin{cases} \frac{r-r^j}{r^{j+1}-r^j} & r > r^j \\ \frac{r-r^j}{r^j-r^{j-1}} & r \leq r^j. \end{cases} \tag{15}$$

Using linear elements for the ion density is however not wise. Indeed for $|\phi_p|/\tau \gg 1$, the convective term in Sys. (7) ($\partial\phi/\partial r/\tau$) becomes large at the probe surface, and a thin ion-density boundary layer which we would need to resolve forms there. Our choice is to use upwind exponential elements:

$$\Psi_i^j(\xi) = \begin{cases} \frac{\exp(\mathrm{Pe}^{j+1})-\exp(\mathrm{Pe}^{j+1}\xi)}{\exp(\mathrm{Pe}^{j+1})-1} & \xi \in [0;1] \\ \frac{\exp(\mathrm{Pe}^{j})-\exp(-\mathrm{Pe}^{j}\xi)}{\exp(\mathrm{Pe}^{j})-1} & \xi \in [-1;0] \\ 0 & \text{otherwise,} \end{cases} \tag{16}$$

where Pe^j and Pe^{j+1} are the numerical Peclet numbers associated with the elements K^j and K^{j+1}:

$$\mathrm{Pe}^j = -\frac{\phi^j - \phi^{j-1}}{\tau} \tag{17}$$

and $\mathrm{Pe}^{j+1} = -(\phi^{j+1} - \phi^j)/\tau$. Using the just-described elements for the ion density allows us not to resolve the ion-density boundary layer if it is thinner than the Debye layer, because those elements are the *exact* solution of the diffusion-mobility equation in one-dimension with uniform advection.

The linear elements (Eq. (14)) can be seen as exponential elements (Eq. (16)) in the limit $\mathrm{Pe} \to 0$; this is consistent with the observation that Poisson's equation is a mobility-diffusion equation with zero mobility. Fig. (1) shows an example of linear and exponential basis functions.

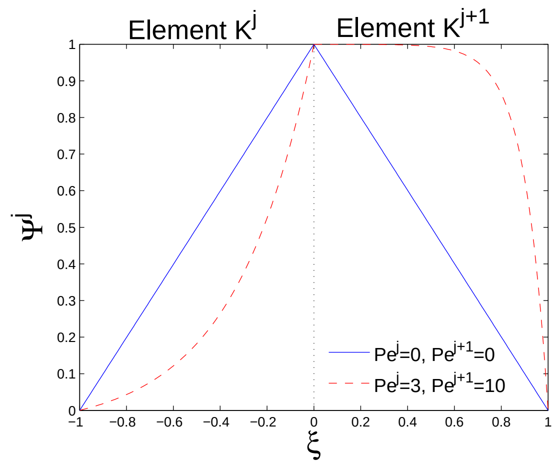

Figure 1: (Color online) Example of linear ($\mathrm{Pe}^j = \mathrm{Pe}^{j+1} = 0$) and exponential ($\mathrm{Pe}^j = 3$ and $\mathrm{Pe}^{j+1} = 10$) basis functions associated with node j, with mobility going from left to right. Numerical Peclet numbers can significantly change from an element to the next if the grid is highly non-uniform.

2.2.2 Equation linearization

Because Sys. (7) is non linear, its solution requires an iterative process. If $n_i^*(r)$ and $\phi_i^*(r)$ are the solutions at the previous iteration, the new (improved) solutions can be found by solving Sys. (7) linearized about n_i^* and ϕ_i^* (i.e. by assuming $|n_i^* - n_i| \ll n_i$ and $|\phi_i^* - \phi_i| \ll |\phi_i|$):

$$\left\{ \begin{array}{lcl} \nabla\left(-\frac{\partial n_i}{\partial r} - \frac{1}{\tau}\left[n_i\frac{\partial \phi^*}{\partial r} + n_i^*\frac{\partial \phi}{\partial r} - n_i^*\frac{\partial \phi^*}{\partial r}\right]\right) & = & 0 \\ \lambda_{De}^2 \nabla\left(\frac{\partial \phi}{\partial r}\right) - \left(n_e^{\mathrm{ext}}(\phi^*, r) + \frac{\partial n_e^{\mathrm{ext}}(\phi^*, r)}{\partial \phi}(\phi - \phi^*) - n_i\right) & = & 0 \end{array} \right. \tag{18}$$

We therefore start with an initial guess for n_i^* and ϕ_i^* (typically uniform $n_i^* = 1$ and Coulomb potential $\phi^* = \phi_p/r$), and repetitively solve Sys. (18) by a standard linear Galerkin approach up to convergence, using the previously described discretization. Of course at each iteration we need to change the basis functions for the ion density Ψ_i^j, according to the latest values of the Peclet numbers.

3 Quasineutral behaviour and regime classification

Following an idea introduced by Su and Lam [8] in the context of small Debye length ($\lambda_{De} \lesssim 1$) CE plasmas, it is convenient to classify the different physical regimes of probe operation according to the quasineutral solutions.

3.1 Quasineutral solutions

The lower-bound ion flux (when the boundary condition $n_{i,e}(r_p) = 0$ is chosen as it is in this paper) is reached when the probe does not induce a potential perturbation in the plasma (i.e. if $\phi_p = 0$ and $\lambda_{De} \to \infty$). It is given by [8]

$$\tilde{\Gamma}_i^0 = N_\infty D_i / R_p = \kappa_i^0 \Gamma_i^0, \tag{19}$$

where $\Gamma_i^0 = N_\infty V_{ti}/(2\sqrt{\pi})$ is the ion thermal flux at infinity, and κ_i^0 an ion Knudsen number.

Similarly the upper-bound electron flux is $\tilde{\Gamma}_e^0 = N_\infty D_e / R_p$ in CE plasmas, and $\Gamma_e^0 = N_\infty D_e^{\mathrm{app}} / R_p$ in KE plasmas.

Far from the probe, Syss (3,7) can easily be solved as a function of the fluxes if Poisson's equation is replaced by quasineutrality ($|n_i - n_e| \ll n_{i,e}$) [8, 9]:

$$\left\{ \begin{array}{lcl} n_{i,e} & = & 1 - \frac{r_s}{r} \\ \phi & = & \eta \ln{(n_{i,e})}. \end{array} \right. \tag{20}$$

We see that $n_{i,e}(r)$ and $\phi(r)$ have a $1/r$ asymptotic dependence as $r \to \infty$, which is fundamentally different from collisionless plasmas where geometric shading effects cause a $1/r^2$ dependence [22].

In CE plasmas (Sys. (3)), r_s and η are given by

$$r_s = \frac{\tau\Gamma_i^p/\tilde{\Gamma}_i^0 + \Gamma_e^p/\tilde{\Gamma}_e^0}{1+\tau} \tag{21}$$

$$\eta = \frac{\tau(\Gamma_i^p/\tilde{\Gamma}_i^0 - \Gamma_e^p/\tilde{\Gamma}_e^0)}{\tau\Gamma_i^p/\tilde{\Gamma}_i^0 + \Gamma_e^p/\tilde{\Gamma}_e^0}, \tag{22}$$

where η is of order unity (unless $|\phi_p| \ll 1$, in which case we will see that $\Gamma_i^p/\tilde{\Gamma}_i^0 \sim \Gamma_e^p/\tilde{\Gamma}_e^0 \sim 1$). r_s is referred to as the sheath radius by Su and Lam [8].

In KE plasmas (Sys. (7)):

$$r_s = \frac{\tau\Gamma_i^p/\tilde{\Gamma}_i^0}{1+\tau} \tag{23}$$

$$\eta = 1. \tag{24}$$

From Eqs (21,23) we see that for CE plasmas $r_s \geq 1$ and for KE plasmas $r_s \geq \tau/(1+\tau)$. The quasineutral CE and KE solutions coincide when $\Gamma_e^p/\tilde{\Gamma}_e^0 \ll \Gamma_i^p/\tilde{\Gamma}_i^0$, in other words when the probe potential ϕ_p is "negative enough".

Two limiting regimes of sheath thickness should be defined:

- Thick sheath: $r_s - 1 \gg 1$.
- Thin sheath: $r_s - 1 \ll 1$.

3.2 Quasineutrality breakdown

The quasineutral solutions (20) are singular at $r = r_s$. As Riemann [23] argued however, the concept of sheath edge defined as the matching point of two asymptotic solutions in $\lambda_{De}/(r-1)$ (presheath) and $(r-1)/\lambda_{De}$ (sheath) should be reserved to purely collisionless plasmas. Indeed here the singularity is never reached, and the quasineutral assumption breaks down at $r \gtrsim r_t$, where we arbitrarily define the transition point r_t by $|\nabla^2\phi(r_t)| = n_{i,e}(r_t)/\lambda_{De}^2$ with ϕ and $n_{i,e}$ given by Eqs (20):

$$\eta\frac{r_s^2}{r_t^4} = \frac{1}{\lambda_{De}^2}\left(1 - \frac{r_s}{r_t}\right)^3, \tag{25}$$

the transition potential $\phi_t = \eta \ln \left(n_{i,e}(r_t)\right)$ being

$$\phi_t = \frac{1}{3}\eta \ln \left(\frac{\eta r_s^2 \lambda_{De}^2}{r_t^4}\right). \tag{26}$$

Solution of Eqs (25,26) in the limit $\eta\lambda_{De}^2/r_s^2 \ll 1$ is

$$\begin{aligned} \frac{r_t}{r_s} &= 1 + \left(\frac{\eta\lambda_{De}^2}{r_s^2}\right)^{1/3} + O\left(\frac{\eta\lambda_{De}^2}{r_s^2}\right)^{2/3} && (27)\\ \phi_t &\sim \frac{1}{3}\eta \ln \left(\frac{\eta\lambda_{De}^2}{r_s^2}\right), && (28) \end{aligned}$$

while in the limit $\eta\lambda_{De}^2/r_s^2 \gg 1$ it is

$$\begin{aligned} \frac{r_t}{r_s} &= \left(\frac{\eta\lambda_{De}^2}{r_s^2}\right)^{1/4} + \frac{3}{4} + O\left(\frac{\eta\lambda_{De}^2}{r_s^2}\right)^{-1/4} && (29)\\ \phi_t &\sim -\eta \left(\frac{\eta\lambda_{De}^2}{r_s^2}\right)^{-1/4}. && (30) \end{aligned}$$

In between, r_t/r_s and ϕ_t are increasing functions of $\eta\lambda_{De}^2/r_s^2$.

Recalling that η is of order one, we will consider the two following limiting regimes in λ_{De}/r_s:

- Strong shielding ("Small Debye length"): $\lambda_{De} \ll r_s$, i.e. $\phi_t \ll -1$.

- Coulomb limit ("Large Debye length"): $\lambda_{De} \gg r_s$, i.e. $|\phi_t| \ll 1$.

The regime $\lambda_{De} \ll r_s$ is referred to as "Strong shielding" because it entails quasineutral solutions extending down to the probe surface, hence $r_s \to 1$.

The limit $\lambda_{De} \gg r_s$ (i.e. $\lambda_{De} \gg r_t$) is referred to as "Coulomb" because in this regime plasma profiles are governed by the quasineutral physics, and become independent of λ_{De}; hence the potential distribution becomes Coulomb ($\phi(r) = \phi_p/r$).

3.3 Probe bias

Extending Su and Lam's classification [8], we define the following bias-regimes:

- Weak bias: $0 \geq \phi_p \gtrsim -\min(1, \tau)$.

- Strong bias: $\phi_p \ll -\max(1,\tau)$ and $\phi_p \lesssim \phi_t$.

- Moderate bias: Otherwise.

3.3.1 Moderate/strong bias transition

It is possible to show that the potential distribution in CE plasmas (with the zero-density inner boundary condition considered in this paper) must be monotonic, therefore regardless of the problem parameters $\phi_t \gtrsim \phi_p$. In the KE regime this is not necessarily true; we can choose $\phi_p \gtrsim \phi_t$, in which case the potential will dip below ϕ_p.

This difference is illustrated in Fig. (2), representing potential profiles calculated with $\tau = 1$, $\lambda_{De} = 10^{-3}$ ($\phi_t \sim 2/3 \ln(10^{-3}) \simeq -4.6$), and two different biases $\phi_p = -1$ and $\phi_p = -4$, for both KE and CE plasmas.

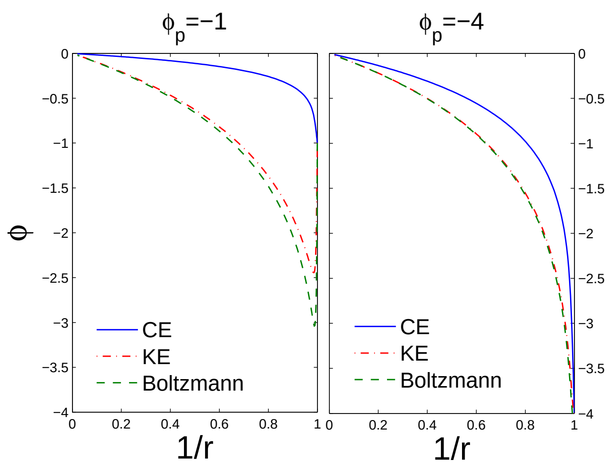

Figure 2: (Color online) Potential profiles plotted against $1/r$, calculated with our numerical code, for $\tau = 1$, $\lambda_{De} = 10^{-3}$ and two different biases $\phi_p = -1$ and $\phi_p = -4$. "CE" curves are solution of Sys. (3), "KE" solution of Sys. (7) with n_e given by Eq. (11), and "Boltzmann" solution of Sys. (7) with n_e given by Eq. (10).

Two observations should be made from Fig. (2). First in situations where the potential distribution is monotonic ($\phi_p = -4$ figure), using the Boltzmann approximation for the kinetic electron density is justified. Second, as $|\phi_p|$ increases the CE and KE potential profiles become closer one to each other. This is consistent with the observation made in Paragraph 3.1 that quasineutral CE and KE solutions are equivalent provided $\Gamma_e^p/\tilde{\Gamma}_e^0 \ll \Gamma_i^p/\tilde{\Gamma}_i^0$.

In fact, it is possible to integrate the electron transport equation in Sys. (3) once, and obtain the electron density profile as a function of the (yet unknown) potential profile as follows (Eq. (2.5) in Ref. [8]):

$$n_e(r) = e^{\phi(r)} \left(1 - \frac{\int_r^\infty \frac{\exp(-\phi(\xi))}{\xi^2}\,\mathrm{d}\xi}{\int_1^\infty \frac{\exp(-\phi(\xi))}{\xi^2}\,\mathrm{d}\xi} \right). \tag{31}$$

For $|\phi_p| \gtrsim O(|\phi_t|) \gg 1$, Su and Lam [8] have shown that Eq. (31) reduces to Eq. (10) down to a distance from the probe surface where $n_e \ll n_i$, hence the precise electron density is not required. This is the strong bias regime, where KE and CE models yield the same potential profiles and the same ion flux density Γ_i^p (The electron flux is of course different).

3.3.2 Weak/moderate bias transition

Su and Lam [8] define a probe as weakly biased when the ion and electron thermal energies are higher than or approximately equal to the electrostatic potential at the probe surface, that is to say $|\phi_p| \lesssim \min(1, \tau)$. This definition is interesting in the context of CE plasmas, because it allows for a linearization of the transport and Poisson's equation about space potential.

However as shown in Fig. (2), for KE plasmas $|\phi_p| \lesssim \min(1, \tau)$ does not imply $|\phi| \lesssim \min(1, \tau)$ everywhere around the probe, hence no distinction between weak and moderate bias is useful.

3.4 Regime classification

We will present our analytic and computational results by subdividing the physical regimes of probe operation as follows:

Table 1: Subdivision of physical regimes considered in this publication.

(1)	Strong shielding, thin sheath	$\lambda_{De} < r_s/10$, $r_s \leq 2$
(2)	Strong shielding, thick sheath	$\lambda_{De} < r_s/10$, $r_s > 2$
(3)	Intermediate shielding	$r_s/10 \leq \lambda_{De} \leq 10 r_s$
(4)	Coulomb limit	$\lambda_{De} > 10 r_s$

The factors "10" and "2" in Tab. 1 might seem arbitrary, but as we will see they define regions in which the corresponding asymptotic solutions are accurate to within 15% or better. Fig. (3) is an illustration of this subdivision in terms of ion density profiles.

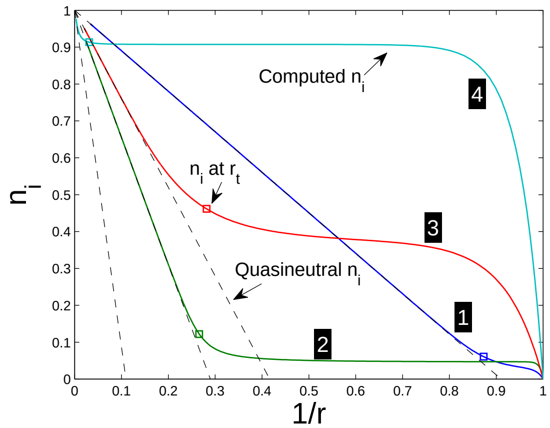

Figure 3: (Color online) Computed ion density profiles for a strongly biased probe with $\tau = 1$, using the following physical parameters: (1) $\lambda_{De} = 0.01$, $\phi_p = -10$; we compute $r_s = 1.098$ and $r_t = 1.14$. (2) $\lambda_{De} = 0.1$, $\phi_p = -100$; we compute $r_s = 3.45$ and $r_t = 3.77$. (3) $\lambda_{De} = 1$, $\phi_p = -10$; we compute $r_s = 2.40$ and $r_t = 3.57$. (4) $\lambda_{De} = 100$, $\phi_p = -20$; we compute $r_s = 9.13$ and $r_t = 32.28$. The dashed lines are the quasineutral solutions (Eq. (20)), and the squares indicate the densities at r_t. For each case r_t is obtained from r_s by solving Eq. (25), r_s being the intersection point of the quasineutral solution with the $n_i = 0$ line. Computations have been performed with the KE equations, but CE calculations would be indistinguishable with such negative ϕ_p.

In the following sections, a series of analytic asymptotic solutions specifically valid in regions 1,2 or 4 of Tab. 1 will be proposed. Those are referenced in Tab. 2.

4 Fluxes with continuum electrons when $|\phi_p| \lesssim 10$

4.1 Analytic solutions

4.1.1 Strong shielding, weak bias

As $\lambda_{De}/r_s \to 0$ at fixed ϕ_p, the quasineutral plasma region extends down to the probe surface and $r_s \to 1$. This is the strong shielding regime, illustrated by the curve (1) in Fig. (3). Injecting $r_s = 1$ in Eqs (21,22) gives

$$\eta = \tau \left(\Gamma_i^p / \tilde{\Gamma}_i^0 - 1 \right) . \tag{32}$$

We can proceed further analytically if $0 \geq \phi_p \gtrsim -\min(1, \tau)$ (weak bias), as Poisson's equation

Table 2: Reference of the major analytic solutions presented in this publication. "*" indicate non straightforwardly new results.

a) Strong shielding regime:

Weak bias CE	Weak/moderate bias KE	Strong bias Thin sheath	Thick sheath
$r_s = 1$	$r_s = 1$	r_s: Eq. (46)*	r_s: Eqs (50,51)*
Γ_i^p: Eq. (37)*	Γ_i^p: Eq. (43)	Γ_i^p: Eq. (47) with Eq. (46)*	Γ_i^p: Eq. (47) with Eqs (50,51)*
Γ_e^p: Eq. (38)*	Γ_e^p: Eq. (8)	$\Gamma_e^p \ll \Gamma_i^p$	$\Gamma_e^p \ll \Gamma_i^p$
ϕ_f: Eq. (53)*	ϕ_f: Eq. (61)	ϕ_f: Eq. (59)*	ϕ_f: Not relevant
c: Eq. (72)*	c: Negative	c: Eq. (73) with Eq. (46)*	c: Eq. (75)*

b) Coulomb regime:

CE plasmas	KE plasmas
r_s: Eq. (21)	r_s: Eq. (23)
Γ_i^p: Eq. (40)	Γ_i^p: Eq. (40)
Γ_e^p: Eq. (42)	Γ_e^p: Eq. (8)
ϕ_f: Eq. (60)	ϕ_f: Eq. (62)
c: Eq. (67)*	c: Eq. (76)*

can then be linearized. Under this hypothesis, Su and Lam (Eq. (6.8) in Ref. [8]) find the potential profile from Sys. (3) as

$$\phi(r) = -\eta \int_{\xi_0}^{\xi_0\left(1-\frac{1}{r}\right)} w(\xi)\ \mathrm{d}\xi, \quad \text{with} \quad \xi_0 = -\lambda_D^{-2/3}, \tag{33}$$

where

$$\lambda_D = \frac{\lambda_{De}}{\sqrt{1+1/\tau}} \tag{34}$$

is the linearized Debye length, and $w(\xi)$ is solution of:

$$\frac{\partial^2 w}{\partial \xi^2} + \xi w + 1 = 0 \tag{35}$$

with boundary conditions $\partial w/\partial \xi(0) = 0$ and $w(-\infty) = 0$.

We first notice from Eq. (35) that in the limit $\xi \ll -1$, $w(\xi) \sim -1/\xi$. Therefore, for $|\xi_0|$ large enough (i.e. in the strong shielding regime), Eq. (33) gives ϕ_p as

$$\phi_p = \phi(1) = -\eta \lim_{A \to -\infty} \left[\int_A^0 w(\xi)\ \mathrm{d}\xi + \ \ln\ \left(\frac{\xi_0}{A} \right) \right]. \tag{36}$$

We solved Eq. (33) numerically with a simple finite difference scheme, and obtain $\lim_{A \to -\infty} \left(\int_A^0 w(\xi)\ \mathrm{d}\xi - \ \ln\ (-A) \right) \simeq 1.356$.

Combining Eqs (32,36) we obtain the ion flux as

$$\frac{\Gamma_i^p}{\tilde{\Gamma}_i^0} = 1 - \frac{\phi_p/\tau}{1.356 - \frac{2}{3}\ \ln\ (\lambda_D)}, \tag{37}$$

and by symmetry the electron flux as

$$\frac{\Gamma_e^p}{\tilde{\Gamma}_e^0} = 1 + \frac{\phi_p}{1.356 - \frac{2}{3}\ \ln\ (\lambda_D)}. \tag{38}$$

Because Su and Lam did not solve Eq. (35), they could only derive the first order expansion in $1/\ \ln\ (\lambda_D)$ of Eq. (37) (Eq. (6.14) in Ref. [8]).

4.1.2 Coulomb limit

In the opposite limit $\lambda_{De}/r_s \to \infty$, the ion and electron dynamics decouple and the potential tends to the Coulomb form $\phi(r) = \phi_p/r$.

Under this assumption, the ion density can be solved for analytically [8]:

$$n_i^{\mathrm{Coul}}(r) = \frac{\exp(-\phi_p/\tau) - \exp\left(-\phi_p/(r\tau)\right)}{\exp(-\phi_p/\tau) - 1}. \tag{39}$$

Injecting the density derivative at the probe edge in Eq. (4), one finds [10]:

$$\frac{\Gamma_i^{p,\mathrm{Coul}}}{\tilde{\Gamma}_i^0} = \frac{\phi_p/\tau}{\exp(\phi_p/\tau) - 1}. \tag{40}$$

By symmetry, the electron density and flux are

$$n_e^{\mathrm{Coul}}(r) = \frac{\exp(\phi_p) - \exp(\phi_p/r)}{\exp(\phi_p) - 1}, \quad (41)$$

$$\frac{\Gamma_e^{p,\mathrm{Coul}}}{\tilde{\Gamma}_e^0} = \frac{\phi_p}{1 - \exp(-\phi_p)}. \quad (42)$$

4.2 Numerical solutions and physical discussion

Figs (4,5) show the collected ion and electron fluxes in CE plasmas as a function of λ_{De}, computed with our numerical code for probe potentials $\phi_p \in [-0.2 : -10]$.

In order to facilitate physical interpretation, the $\Gamma_{i,e}^p - \lambda_{De}$ space is divided by brown dash-dot lines in the four regions defined in Tab. 1. Region (1) is further subdivided in (1b), with $r_s \leq 1.1$.

Eqs (37,38) are applicable for $\lambda_{De} \ll r_s$ and $r_s = 1$, corresponding (to within 10%) to region (1b). Although they formally require $|\phi_p| \ll \min(1, \tau)$, Fig. (4) shows that $\phi_p \gtrsim -5$ is sufficient to have less than 10% error on Γ_i^p; the error on Γ_e^p is a little higher. Nevertheless it is clear that as $\phi_p \to 0$ the asymptotic formula matches the numerical solution.

As noticed by Baum and Chapkis [10], at fixed ϕ_p we see that $\Gamma_{i,e}^p / \tilde{\Gamma}_{i,e}^0 \to 1$ as $\lambda_{De} \to 0$. Even at $\lambda_{De} = 10^{-5}$ however, the fluxes are not yet saturated.

In region (4), corresponding to the Coulomb regime, the ion and electron fluxes tend as expected to the prediction of Eqs (40,42).

5 Fluxes with kinetic electrons when $|\phi_p| \lesssim 10$

5.1 Analytic solutions

As for CE plasmas, the KE strong shielding limit is characterized by $r_s \to 1$. Using Eq. (23) with $r_s = 1$, we straightforwardly obtain

$$\frac{\Gamma_i^p}{\tilde{\Gamma}_i^0} = \frac{1+\tau}{\tau}. \quad (43)$$

a) $\tau = 1$

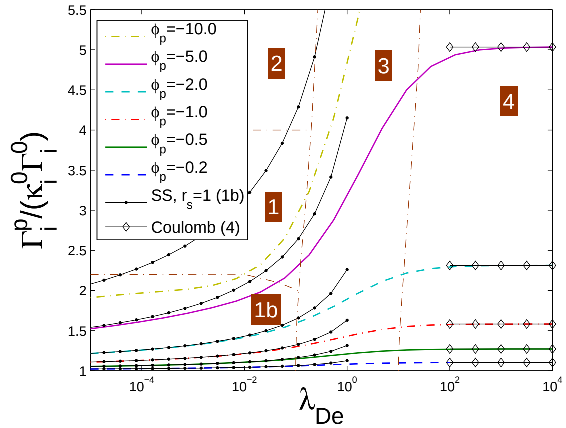

b) $\tau = 0.1$

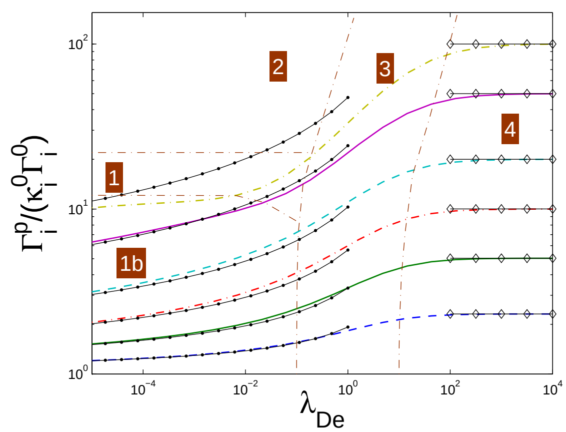

Figure 4: (Color online) Evolution of the collected ion flux Γ_i^p (normalized to $\tilde{\Gamma}_i^0 = \kappa_i^0 \Gamma_i^0 = N_\infty D_i / R_p$) with λ_{De} in CE plasmas, for $\tau = 1$ (a) and $\tau = 0.1$ (b). "$SS, r_s = 1$" curves correspond to Eq. (37), and "Coulomb" asymptotes to Eq. (40). The $\Gamma_i^p - \lambda_{De}$ space is divided in four regions corresponding to the regimes described in Tab. 1. Region "(1b)" is a subsection of region (1) with $1 \leq r_s \leq 1.1$.

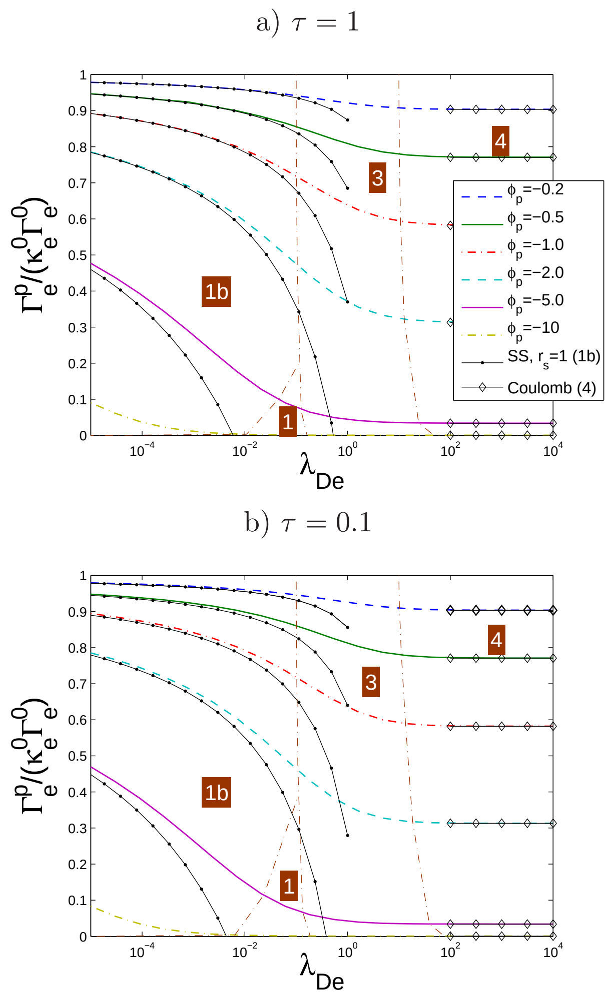

Figure 5: (Color online) Evolution of the collected electron flux Γ_e^p (normalized to $\tilde{\Gamma}_e^0 = \kappa_e^0\Gamma_e^0 = N_\infty D_e/R_p$) with λ_{De} in CE plasmas, for $\tau = 1$ (a) and $\tau = 0.1$ (b). "$SS, r_s = 1$" curves correspond to Eq. (38), and "Coulomb" asymptotes to Eq. (42). The $\Gamma_e^p - \lambda_{De}$ space is divided as in Fig. (4).

Contrary to the derivation of Eq. (37), no weak-bias assumption is used here, since Poisson's equation need not be solved.

The Coulomb limit ion results (Eqs (39,40)) are still valid for KE plasmas.

5.2 Numerical solutions and physical discussion

Fig. (6) shows the collected ion flux in KE plasmas as a function of λ_{De}, computed with our numerical code for probe potentials $\phi_p \in [-0.2 : -5]$.

Dotted portions of curves correspond to parameters where the potential profile dips below ϕ_p, hence we need to rely on our extended model (Eq. (11)) for which we do not claim any accuracy. This regime would however be worth further analysis since we find the unintuitive result that the flux decreases with increasing Debye length, and more interestingly we will see in Section 10 that there the probe capacitance is negative.

As $\lambda_{De} \to 0$, the ion flux tends to the strong-shielding asymptote predicted by Eq. (43). In region (1), Eq. (43) is accurate to within 15% for the $\phi_p = -5$ curves.

In region (4), corresponding to the Coulomb regime, the ion flux tends as expected to the prediction of Eq. (40).

6 Fluxes when $\phi_p \leq -10$

The strong shielding transition potential at $\lambda_{De} = 10^{-5}$ is $\phi_t \sim -7$ (Eq. (28) with $r_s \sim 1$), hence the choice $\phi_p \leq -10$ guarantees that for $\lambda_{De} \gtrsim 10^{-5}$ probes operate in the strong bias regime. Considering $\lambda_{De} \lesssim 10^{-5}$ would not be reasonable, since for a typical probe with $R_p \sim 1$mm, we would approach quantum conditions.

In this section devoted to the strong bias regime we shall therefore not distinguish between CE and KE plasmas. Numerical results presented here derive from KE calculations with n_e given by Eq. (10), but using Eq. (6) (or even assuming a CE plasma) would be equivalent.

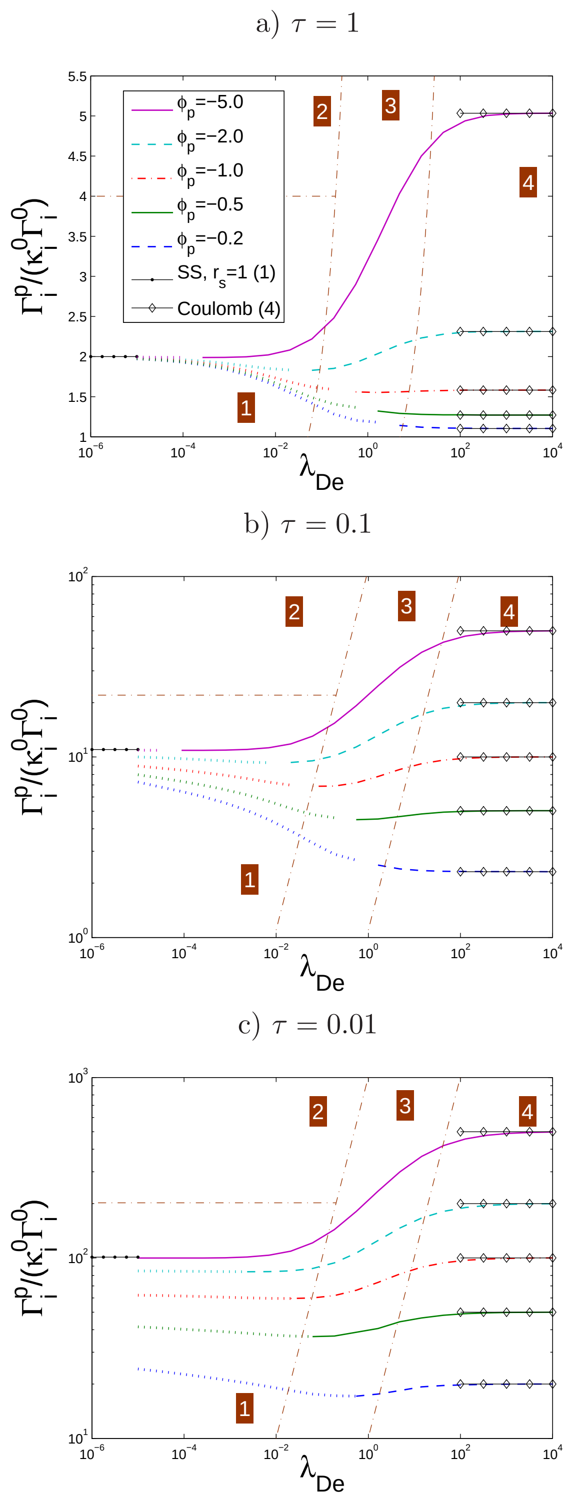

Figure 6: (Color online) Evolution of the collected ion flux Γ_i^p (normalized to $\tilde{\Gamma}_i^0 = \kappa_i^0\Gamma_i^0 = N_\infty D_i/R_p$) with λ_{De} in KE plasmas, for $\tau = 1$ (a), $\tau = 0.1$ (b) and $\tau = 0.01$ (c). Solid lines correspond to regions of $\lambda_{De} - \phi_p$ space where the potential profiles are monotonic (hence n_e is given by Eq. (6)). Dotted lines correspond to regions of $\lambda_{De} - \phi_p$ space where the potential profiles have a dip below ϕ_p (calculations have been performed with n_e given by Eq. (11)). "$SS, r_s = 1$" asymptotes correspond to Eq. (43), and "Coulomb" asymptotes to Eq. (40). The $\Gamma_i^p - \lambda_{De}$ space is divided in four regions corresponding to the regimes described in Tab. 1.

6.1 Analytic solutions

6.1.1 Strong shielding, thin sheath

In the strong bias regime, Su and Lam (Eq. (3.23a) from Ref. [8]) took advantage of the Boltzmann distribution of the electrons and assumed $\lambda_{De}/r_s \ll 1$ to derive the following expression for the potential distribution in the sheath ($r < r_s$):

$$\phi(r) = \frac{2}{3}\ \ln\ \left(\frac{\lambda_{De}}{r_s\sqrt{1+\tau}}\right) - c(\tau) - \sqrt{\frac{2}{3}}\left(\frac{\sqrt{1+\tau}}{\lambda_{De}}\right)\int_r^{r_s}\left[1-\left(\frac{x}{r_s}\right)^3\right]^{1/2}\left(\frac{r_s}{x}\right)^2\ \mathrm{d}x. \tag{44}$$

In Eq. (44), $c(\tau)$ is a weakly varying function of τ ($c(\tau) \simeq 3$). Two interesting limits of Eq. (44) are the thin and thick sheath regimes.

In the thin sheath limit ($r_s - 1 \ll 1$) one can let $r_s = 1 + \epsilon_s$ with $\epsilon_s \ll 1$ in Eq. (44). If we further set $r = r_p = 1$, to order $\epsilon_s^{3/2}$ Eq. (44) reads:

$$\phi_p = \frac{2}{3}\ \ln\ \left(\frac{\lambda_{De}}{\sqrt{1+\tau}}\right) - c(\tau) - \frac{2\sqrt{2}}{3}\frac{\sqrt{1+\tau}}{\lambda_{De}}\epsilon_s^{3/2} - \frac{2}{3}\epsilon_s. \tag{45}$$

Rigorously, in Eq. (45) the "$\epsilon_s^{3/2}$" term has a higher order than the "ϵ_s" term. However recall that we are in the strong bias regime, hence $|\phi_p|$ is much larger than $|\ \ln\ \left(\lambda_{De}/\sqrt{1+\tau}\right)|$ and unity. Since $\epsilon_s \ll 1$, the factor in front of $\epsilon_s^{3/2}$ must be very large. It is therefore appropriate to drop the "ϵ_s" term in Eq. (45).

The strong bias, thin sheath, strong shielding sheath radius is therefore:

$$r_s = 1 + \left[\frac{3}{2\sqrt{2}}\frac{\lambda_{De}}{\sqrt{1+\tau}}\left(\frac{2}{3}\ \ln\ \left(\frac{\lambda_{De}}{\sqrt{1+\tau}}\right) - \phi_p - c(\tau)\right)\right]^{2/3}. \tag{46}$$

Eq. (46) breaks down when $|\phi_p| < c(\tau) - 2/3\ \ln\ \left(\lambda_{De}/\sqrt{1+\tau}\right)$, indicating that we leave the strong bias regime.

The ion flux is then given by inversion of Eq. (23) (KE plasmas) or Eq. (21) with $\Gamma_e^p/\tilde{\Gamma}_e^0 \ll \Gamma_i^p/\tilde{\Gamma}_i^0$ (CE plasmas):

$$\Gamma_i^p/\tilde{\Gamma}_i^0 = \frac{1+\tau}{\tau} r_s. \tag{47}$$

For completeness, we point that in the limit $|\phi_p| \gg \max\left(c(\tau), -\ \ln\ \left(\lambda_{De}/\sqrt{1+\tau}\right)\right)$, in practice $|\phi_p| \gtrsim 50$, Eq. (46) simplifies to

$$r_s = 1 + \left(-\frac{3}{2\sqrt{2}}\frac{\phi_p \lambda_{De}}{\sqrt{1+\tau}}\right)^{2/3}. \tag{48}$$

The $r_s - 1 \propto (-\phi_p \lambda_{De})^{2/3}$ dependence for $r_s - 1 \ll 1$ had been anticipated by Brailsford (Eq. (16) in Ref. [24]) by means of a heuristic model, unfortunately he finds the incorrect coefficient.

6.1.2 Strong shielding, thick sheath

When the thick sheath limit ($r_s - 1 \gg 1$) of Eq. (44) is reached, the potential at the sheath entrance $\phi(r_s)$ is negligible compared to ϕ_p. In this case we can drop the first two terms on the right hand side of Eq. (44). If we set $r = r_p = 1$, we recover Kiel's Ohmic model derived with a quite different approach [12]:

$$r_s^2 \int_1^{r_s} \left[1 - \left(\frac{x}{r_s}\right)^3\right]^{1/2} \frac{\mathrm{d}x}{x^2} = \gamma_1, \tag{49}$$

where

$$\gamma_1 = -\phi_p \lambda_{De} \left[\frac{3}{2(1+\tau)}\right]^{1/2}. \tag{50}$$

Expanding Eq. (49) for large γ_1 to order 0(1):

$$r_s = \sqrt{\gamma_1} + \frac{5}{8}. \tag{51}$$

In other words, as already pointed out by Su and Lam, at fixed λ_{De} when $|\phi_p| \to \infty$ the ion flux varies as $\Gamma_i^p \propto (-\phi_p \lambda_{De})^{1/2}$. This result has erroneously been contradicted by authors basing their argument on incomplete current-voltage characteristics. This is for instance the case of Cicerone and Bowhill [11] (Numerical simulation) or Kamitsuma and Chen [5] (Experiment) who conclude in a flux dependence for strongly biased probes of the form $\Gamma_i^p \propto (-\phi_p)^s$ where s is a function of λ_{De}.

After integrating Eq. (49) numerically for $\gamma_1 \in [1:500]$, and enforcing $r_s = 1$ for $\lambda_{De}|\phi_p| \ll 1$, Kiel proposes the following approximate form for the sheath radius:

$$r_s = \left[1 + 0.83\gamma_1^{0.535}\right] . \tag{52}$$

Eq. (52) is only approximate, as it does not match Eq. (46) when $\gamma_1 \ll 1$ or Eq. (51) when $\gamma_1 \gg 1$.

6.1.3 Coulomb limit

Eq. (44) breaks down when λ_{De} approaches the order of r_s. In the opposite limit of $\lambda_{De} \gg r_s$, the Coulomb limit solution (Eq. (40)) applies.

6.2 Numerical solutions and physical discussion

6.2.1 Flux dependence on λ_{De}

Fig. (7) shows the evolution of the ion flux-density to the probe, computed with our numerical code in the strong bias regime, as a function of λ_{De}.

Superposition of the "exact" solutions with the analytic asymptotic curves is of course perfect in their respective limits. It is however interesting to notice that using Eq. (46) in the entire region (1), Eqs (50,51) in the entire region (2), and Eq. (40) in the entire region (4) yields less than 15% error on the ion flux. In other words, except in region (3) where there is no convenient asymptotic expansion, we solved the continuum probe problem to within typical experimental accuracy.

The curves at $\phi_p = -10$ in Fig. (7) are identical to those plotted in Fig. (4), except for $\lambda_{De} \lesssim 10^{-5}$ where we transition to the moderate bias regime, hence KE and CE calculations differ.

We emphasize here that the Coulomb limit results for the fluxes are valid for $\lambda_{De} \gg r_s$, which is more stringent than the usually assumed condition $\lambda_{De} \gg r_p = 1$.

6.2.2 Current-voltage characteristics

Fig. (8) shows the current-voltage characteristics for $\tau = 1$, $\tau = 0.1$ and $\tau = 0.01$ when $|\phi_p| \geq 10$ as computed by our numerical code. For clarity, we did not superpose the corresponding analytic

a) $\tau = 1$

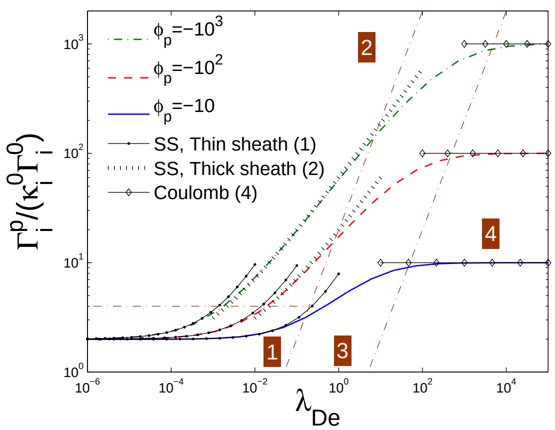

b) $\tau = 0.1$

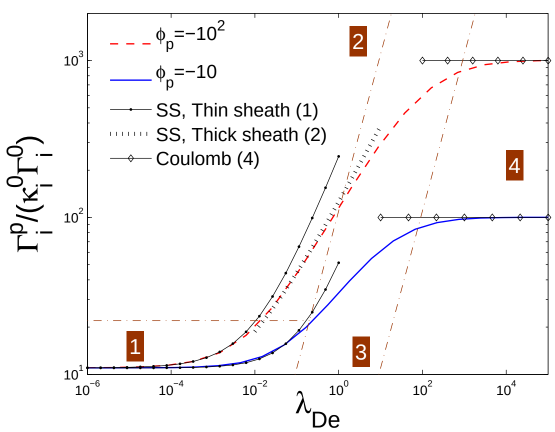

Figure 7: (Color online) Evolution of the ion flux density (normalized to $\tilde{\Gamma}_i^0 = \kappa_i^0 \Gamma_i^0 = N_\infty D_i / R_p$) with the electron Debye length for $\tau = 1$ (a) and $\tau = 0.1$ (b), in the strong bias regime. The $\Gamma_i^p - \lambda_{De}$ space is divided in four regions corresponding to the regimes described in Tab. 1. "SS, Thin sheath" (region 1) and "SS, Thick sheath" (region 2) curves correspond to Eq. (47) with r_s respectively given by Eq. (46) and Eqs (50,51). "Coulomb" (region 4) asymptotes correspond to Eq. (40).

solutions.

It is convenient to analyze Fig. (8) at fixed ϕ_p, from large to small λ_{De}. In the limit $\lambda_{De} = \infty$, the ion flux density is given by the Coulomb calculation (Eq. (40)), according to which the ion flux is $\Gamma_i^p \propto -\phi_p$ in the considered strong bias regime. This is region (4). As λ_{De} decreases we enter the intermediate shielding regime, region (3). As λ_{De} is further reduced, we enter the strong shielding, thick sheath regime (region (2)), where the ion flux is given by Eq. (47) with Eqs (50,51). For small enough λ_{De} the sheath radius becomes smaller than $r_s = 2$ and we reach the strong shielding, thin sheath regime (region (1)) where the ion flux is given by Eq. (47) with Eq. (46).

7 Floating potential solutions with Continuum electrons

7.1 Analytic solutions

7.1.1 Strong shielding, weak bias

The CE floating potential in the strong shielding, weak bias regime ($r_s = 1$) is straightforwardly given by equating Eq. (37) to Eq. (38):

$$\phi_f = \frac{1 - D_e/D_i}{D_e/D_i + 1/\tau}\left(1.356 - \frac{2}{3}\ln\,(\lambda_D)\right). \tag{53}$$

By normalizing ion (electron) fluxes to $\tilde{\Gamma}_i^0$ ($\tilde{\Gamma}_e^0$ or Γ_e^0), diffusivities can be simplified out from Syss (3,7), explaining why in the previous sections diffusivities did not explicitly appear in the solutions. Diffusivity ratios (D_e/D_i or D_e^{app}/D_i in the next section) here appear as a key parameter governing floating potentials.

7.1.2 Strong shielding, strong bias (thin sheath)

In Section 6, we did not present electron flux results. Indeed double machine precision is 2^{-53}, hence electron fluxes scaling as $\exp(\phi_p)$ can not directly be calculated when $\phi_p \lesssim -30$. Γ_e^p is nevertheless required for floating potential calculations.

Recalling that $\Gamma_e^p = \tilde{\Gamma}_e^0 \partial n_e/\partial r(r_p)$, the electron flux can be obtained by differentiation of Eq. (31)

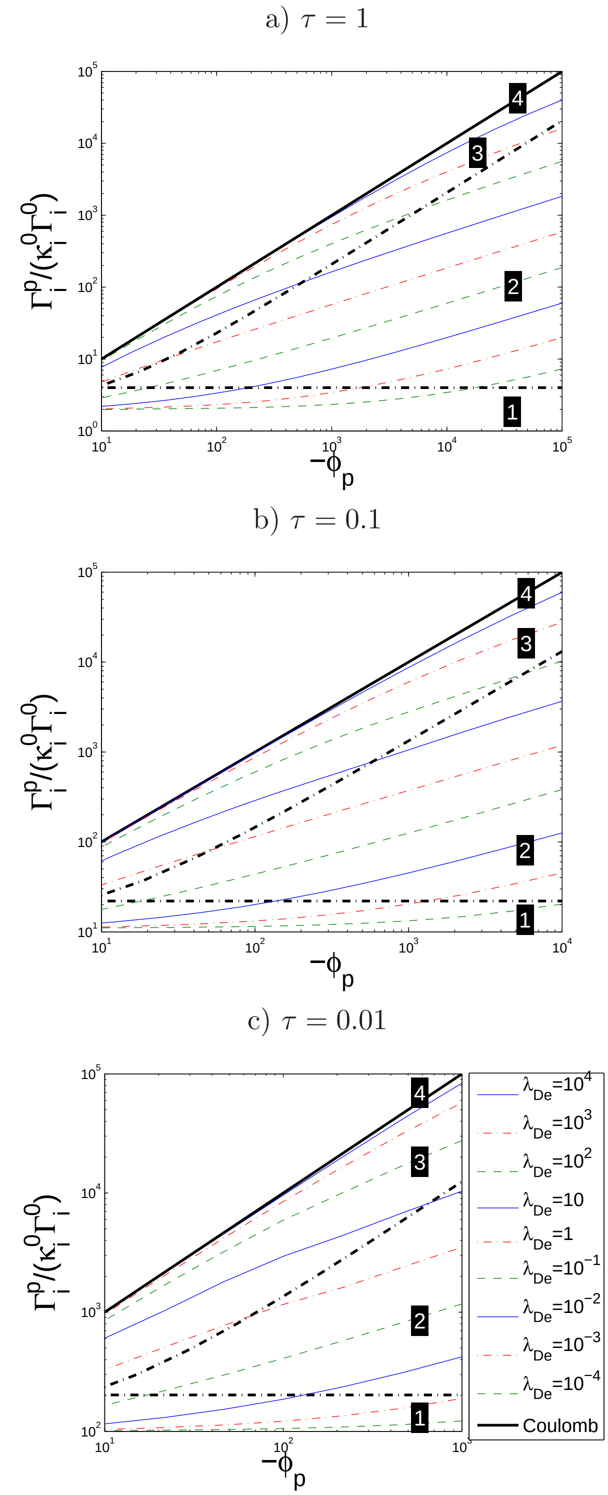

Figure 8: (Color online) Current-voltage characteristics for $\tau = 1$ (a), $\tau = 0.1$ (b) and $\tau = 0.01$ (c), for $|\phi_p| \geq 10$. The ion flux density is normalized to $\tilde{\Gamma}_i^0 = \kappa_i^0 \Gamma_i^0 = N_\infty D_i / R_p$. The four regions of $r_s - \lambda_{De}$ space described in Tab. 1 are mapped to the $\Gamma_i^p - \phi_p$ space, hence region (4) is degenerate with the "Coulomb" solution (Eq. (40)).

at $r = r_p = 1$. This yields (Eq. (2.6) in Ref. [8]):

$$\frac{\Gamma_e^p}{\tilde{\Gamma}_e^0} = \left[\int_1^\infty \frac{\exp\left(-\phi(\xi)\right)}{\xi^2}\,\mathrm{d}\xi\right]^{-1}. \tag{54}$$

The potential profile $\phi(r)$ around a strong bias floating probe ($\Gamma_e^p = \Gamma_i^p$ with $\Gamma_i^p/\tilde{\Gamma}_i^0$ given by Eq. (47)) must therefore satisfy the following equation:

$$\frac{\tau D_e}{(1+\tau)D_i} = r_s \int_1^\infty \frac{\exp\left(-\phi(\xi)\right)}{\xi^2}\,\mathrm{d}\xi. \tag{55}$$

Because $\lambda_{De} \ll r_s$ (strong shielding), most of the potential drop occurs within $r = 1$ and $r = r_s$ (i.e. $|\phi(r_s)| \ll |\phi_f|$). In addition, our numerical solutions will show that for physically reasonable parameters the floating potential is $|\phi_f| \lesssim 0(10)$; hence in the strong shielding, strong bias regime, we operate in region (1) of Tab. 1 and $r_s - 1 \ll 1$ (thin sheath).

We can therefore set $\phi(r) = \phi_f + (r-1)\partial\phi/\partial r(1)$ in Eq. (55), and integrate between $r = 1$ and $r = r_s \sim 1$, yielding

$$\frac{\tau D_e}{(1+\tau)D_i} = r_s \exp(-\phi_f)\left[\frac{\partial\phi}{\partial r}(1)\right]^{-1}. \tag{56}$$

Differentiation of Eq. (44) with respect to r at $r = r_p = 1$ yields:

$$\frac{\partial\phi}{\partial r}(1) = \sqrt{\frac{2}{3}}\left(\frac{\sqrt{1+\tau}}{\lambda_{De}}\right)\left[1 - \frac{1}{r_s^3}\right]^{1/2} r_s^2. \tag{57}$$

In the thin sheath limit ($r_s - 1 \ll 1$):

$$\frac{\partial\phi}{\partial r}(1) = \frac{\sqrt{2(1+\tau)}}{\lambda_{De}}\sqrt{r_s - 1}, \tag{58}$$

where r_s is given by Eq. (46).

Eq. (56) with $\partial\phi/\partial r(1)$ given by Eq. (58) can be solved explicitly if $|\phi_f/\ln(\phi_f)| \gg 1$ is assumed:

$$\phi_f = -\ln\left(\frac{\tau D_e}{(\tau+1)D_i}\right) + \frac{2}{3}\ln\left(\frac{\lambda_{De}}{\sqrt{1+\tau}}\right) - \frac{1}{3}\ln\left[3\left(\ln\left(\frac{\tau D_e}{(\tau+1)D_i}\right) - c(\tau)\right)\right]. \tag{59}$$

7.1.3 Coulomb limit

Analytic expressions for the floating potential in the Coulomb limit can be calculated by equating Eq. (40) to Eq. (42):

$$D_i \frac{\phi_f/\tau}{\exp(\phi_f/\tau) - 1} = D_e \frac{\phi_f}{1 - \exp(-\phi_f)}. \tag{60}$$

Eq. (60) can be solved explicitly when $\tau = 1$, yielding $\phi_f = -\ln\,(D_e/D_i)$. For arbitrary temperature ratio τ, $\phi_f \to -\ln\,(\tau D_e/D_i)$ in the limit $|\phi_f| \gg \max(1, \tau)$.

7.2 Numerical solutions and physical discussion

Fig. (9) shows the probe floating potential as a function of λ_{De} in CE plasmas.

It can be seen that at fixed λ_{De}, $|\phi_f|$ increases with D_e/D_i. Indeed for lower ion diffusivity, stronger probe bias is required for the ion flux to match the electron's. Similarly, at fixed diffusivity ratio D_e/D_i, $|\phi_f|$ increases for decreasing λ_{De}.

In the strong shielding regime, the weak bias solution (Eq. (53)) applies when $\phi_f \gtrsim -5$, which is very fortunate as we recall that it formally requires $|\phi_f| \ll \min(1, \tau)$. When $\phi_f \lesssim -10$, the strong bias solution (Eq. (59)) applies.

In the Coulomb limit, ϕ_f tends to the value predicted by Eq. (60).

8 Floating potential solutions with Kinetic electrons

8.1 Analytic solutions

In KE plasmas, the floating potential in the strong shielding regime is given by equating Eq. (43) to Eq. (8):

$$\phi_f = -\ln\left(\frac{\tau}{1+\tau}\frac{D_e^{\mathrm{app}}}{D_i}\right). \tag{61}$$

Of course Eq. (61) is valid provided Eq. (8) can be used, in other words with the assumption that no dip below ϕ_p forms in the potential profile (such as in Fig. (2a) for instance).

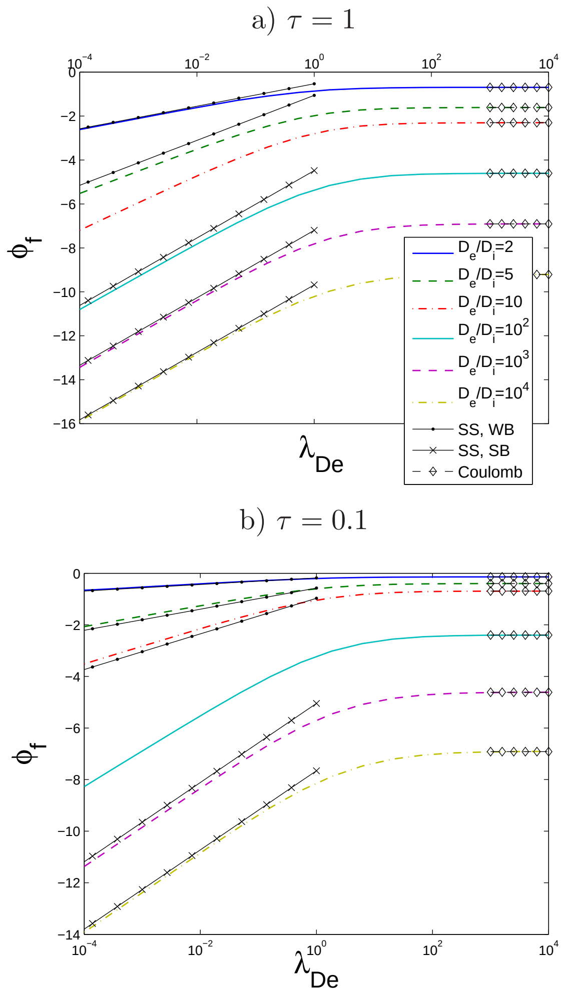

Figure 9: (Color online) Probe floating potential in CE plasmas as a function of λ_{De} for $\tau = 1$ (a) and $\tau = 0.1$ (b). A wide range of diffusivity ratios is explored ($D_e/D_i \in [2 : 10^4]$). "SS, WB" curves correspond to the strong shielding, weak bias solutions (Eq. (53)), "SS, SB" curves to the strong shielding, strong bias solutions (Eq. (59)) and the "Coulomb" asymptotes to the solution of Eq. (60). When ϕ_f is approximately between -5 and -10, none of the two strong shielding formulas apply.

In the Coulomb limit, the floating potential can be calculated by equating Eq. (40) to Eq. (8):

$$D_i \frac{\phi_p/\tau}{\exp(\phi_p/\tau) - 1} = D_e^{\text{app}} \exp(\phi_p). \tag{62}$$

8.1.1 Numerical solutions and physical discussion

Fig. (10) shows the probe floating potential as a function of λ_{De} in KE plasmas.

In the large Debye length limit ϕ_f tends to the value predicted by Eq. (62), but contrary to the CE regime ϕ_f does tend to a limit when $\lambda_{De} \ll r_s$ (Eq. (61)), at least as long as the potential profiles are monotonic.

Indeed when $\phi_t \lesssim \phi_f$ and a potential well forms around the probe, decreasing λ_{De} at fixed ϕ_p decreases the electron flux (according to the model extension in Paragraph. 2.1.2), hence increases the floating potential. As we do not claim any accuracy in our results when the potential profiles are not monotonic, we do not elaborate further.

9 Capacitance with Continuum electrons

9.1 Analytic solutions

9.1.1 Coulomb limit

In a series of recent publications (see for instance [18] and references herein), Khrapak *et al* have investigated Syss (3,7) by linearizing the mobility-diffusion and Poisson's equations about the unperturbed plasma density and potential, and assuming $\lambda_D \gg 1$ (Eq. (34)). Their model yields the following potential distribution:

$$\phi(r) = \frac{\phi_p}{r} \exp\left(-\frac{r-1}{\lambda_D}\right) - \frac{r_s \eta}{r}\left[1 - \exp\left(-\frac{r-1}{\lambda_D}\right)\right], \tag{63}$$

where r_s and η are given by Eqs (21,22) or Eqs (23,24). When $r \to \infty$, one recovers Eq. (20) as expected.

Eq. (63) can be applied when the Debye length is longer than the distance it takes for the potential to satisfy $|\phi| \ll \min(1, \tau)$, i.e. $\lambda_{De} \gg |\phi_p|/\min(1, \tau)$, in addition to $\lambda_{De} \gg 1$. Indeed

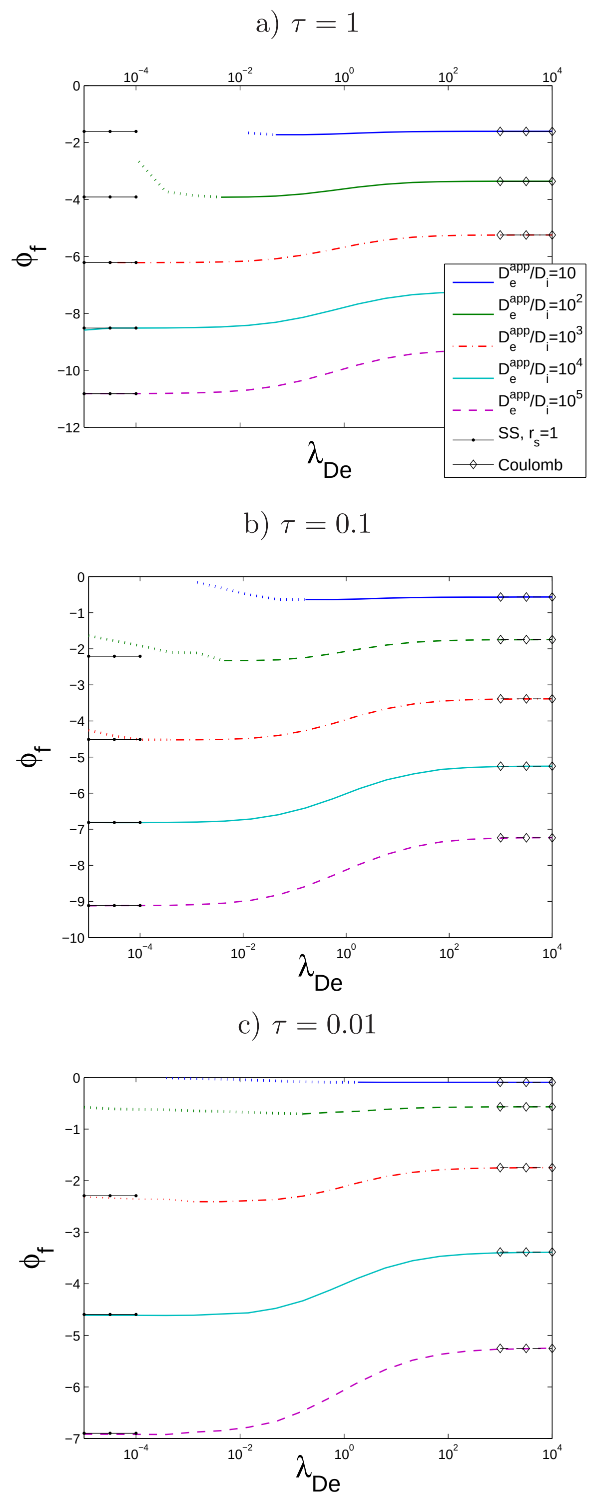

Figure 10: (Color online) Probe floating potential in KE plasmas as a function of λ_{De} for $\tau = 1$ (a), $\tau = 0.1$ (b) and $\tau = 0.01$ (c). A wide range of diffusivity ratios is explored ($D_e^{\text{app}}/D_i \in [10 : 10^5]$). "SS, $r_s = 1$" asymptotes correspond to Eq. (61), and "Coulomb" asymptotes to Eq. (62). Dotted portions of curves correspond to $\phi_f - \lambda_{De}$ parameter space where the potential profiles are not monotonic, hence we can not assert the accuracy of our results.

when this condition is satisfied, although a linearized treatment is not appropriate in the vicinity of the probe, the potential slope there is determined by the ion and electron density distributions in a few Debye spheres from there where the potential and density perturbations are indeed "small".

Eq. (63) was first published by Su and Lam (last unlabeled equation, following Eq. (A11) in Ref. [8]), but their approach to its derivation was quite different and no physical discussion of the formula was given. In addition, the linear approach of Ref. [18] allows to treat weakly drifting plasmas, although not required here.

In both Refs [8, 18], Eq. (63) is proposed with $\exp(-r/\lambda_D)$ instead of $\exp(-(r-1)/\lambda_D)$. Because it is first order in $1/\lambda_D$ both forms are equally valid, but Eq. (63) is more convenient as it gives the correct potential for $r = r_p = 1$.

Perhaps the most useful usage of Eq. (63) is to extract the dimensionless probe capacitance

$$c = -\frac{1}{\phi_p}\frac{\partial \phi}{\partial r}(1), \tag{64}$$

the dimensional capacitance being $C = 4\pi\epsilon_0 R_p c$, and the dimensional probe charge

$$Q_p = CV_p. \tag{65}$$

We obtain

$$c^{\mathrm{Coul}} = 1 + \frac{1}{\lambda_D}\left(1 + \frac{r_s\eta}{\phi_p}\right). \tag{66}$$

Eq. (66) readily shows that collisions decrease the capacitance from the large Debye length collisionless value $c = (1 + 1/\lambda_D)$ [25], since $\phi_p \leq 0$ and $r_s\eta \geq 0$.

The condition $\lambda_{De} \gg |\phi_p|/\min(1,\tau)$ implies $\lambda_{De}/r_s \gg 1$ (see Fig. (8)), hence we can calculate $r_s\eta$ using the expressions for the ion and electron fluxes in the Coulomb limit (Eqs (40,42) in the CE regime):

$$c^{\mathrm{Coul}} = 1 + \frac{1}{\lambda_D}\left[1 + \frac{\tau}{1+\tau}\left(\frac{1/\tau}{\exp(\phi_p/\tau) - 1} - \frac{1}{1 - \exp(-\phi_p)}\right)\right]. \tag{67}$$

For $|\phi_p| \lesssim 2\min(1,\tau)$, c^{Coul} reads

$$c^{\text{Coul}} = 1 + \frac{1}{\lambda_D}\left[\frac{1}{2} - \frac{\phi_p}{12}\frac{\tau-1}{\tau}\right], \tag{68}$$

while for $|\phi_p| \gtrsim 2\max(1,\tau)$, c^{Coul} reads

$$c^{\text{Coul}} = 1 + \frac{\tau}{1+\tau}\frac{1}{\lambda_D}. \tag{69}$$

When $\tau = 1$, Eq. (67) takes the following very simple form, independent of ϕ_p:

$$c^{\text{Coul}} = 1 + \frac{1}{2\lambda_D}. \tag{70}$$

9.1.2 Weak bias, strong shielding

In the weak bias, strong shielding limit, we can use Eq. (33) to write

$$\frac{\partial\phi}{\partial r}(1) = \frac{\partial\phi}{\partial\xi}\frac{\partial\xi}{\partial r}(1) = -\eta w(0)\xi_0; \tag{71}$$

our numerical solution of Eq. (33) gives $w(0) = 1.288$.

Replacing η with Eqs (32,37), we find an analytic formula for the dimensionless probe capacitance, valid for $\lambda_{De} \ll r_s$ and $|\phi_p| \lesssim \min(1,\tau)$ (formally $|\phi_p| \ll \min(1,\tau)$):

$$c = \frac{1.288}{\lambda_D^{2/3}\left(1.356 - \frac{2}{3}\ln\left(\lambda_D\right)\right)}, \tag{72}$$

where again λ_D is the linearized Debye length (Eq. (34)). Because deriving from a linear treatment of Poisson's equation, Eq. (72) is independent of ϕ_p.

9.1.3 Strong bias, strong shielding, thin sheath

Differentiation of Eq. (44), valid in the strong shielding and strong bias regime, with respect to r at $r = r_p = 1$ in the thin sheath limit ($r_s = 1 + \epsilon_s$ with $\epsilon_s \ll 1$), has previously been performed in the context of floating potential calculations (Eq. (58)). It readily yields the capacitance as

$$c = -\sqrt{2(1+\tau)}\frac{\sqrt{r_s - 1}}{\phi_p \lambda_{De}}, \tag{73}$$

with r_s given by Eq. (46).

When $\phi_p \lesssim -50$, we can use Eq. (48) and the capacitance simplifies to:

$$c = 3^{1/3}\left(-\frac{1+\tau}{\lambda_{De}\phi_p}\right)^{2/3}. \tag{74}$$

9.1.4 Strong bias, strong shielding, thick sheath

In the opposite limit of thick sheath (but still strong bias and strong shielding), combination of Eqs (51,57) yields

$$c = 1 + \frac{5}{4}\left[\frac{2(1+\tau)}{3}\right]^{1/4} \frac{1}{\sqrt{-\phi_p \lambda_{De}}}. \tag{75}$$

9.2 Numerical solutions and physical discussion

Figs (11,12) show the probe dimensionless capacitance defined by Eq. (64) as a function of λ_{De} for CE plasmas. For convenience $c-1$ is plotted, and the weak/moderate and strong bias results are shown separately.

Plasmas with $\tau = 1$ have the interesting property of having a capacitance quasi independent of ϕ_p for $|\phi_p| \lesssim 10$ (Fig. (11a)). Indeed both the equithermal Coulomb capacitance (Eq. (70)) and the weak bias, strong shielding capacitance (Eq. (72)) are independent of ϕ_p.

Fig. (11b) shows that this is not the case for plasmas with $\tau < 1$. The general Coulomb capacitance (Eq. (67)) depends on ϕ_p, and the weak bias, strong shielding capacitance is only valid for $|\phi_p|/\min(1,\tau) \lesssim 10$ (this is fortunate as the formal condition is $|\phi_p|/\min(1,\tau) \ll 1$), i.e. $|\phi_p| \lesssim -1$ if $\tau = 0.1$.

Capacitances for $\phi_p \leq -10$ are plotted in Fig. (12), and show perfect agreement with the strong shielding (Eq. (73) and Eq. (75)) and Coulomb solutions in their regime of validity, i.e. respectively region 1, 2 and 4 of Tab. 1.

Two trends are clearly observable. First c increases with decreasing λ_{De}, in agreement with

a) $\tau = 1$

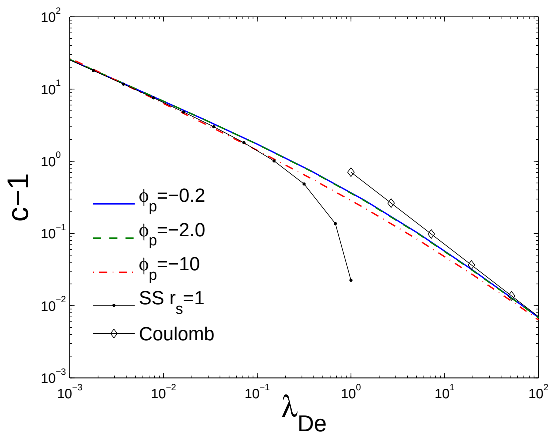

b) $\tau = 0.1$

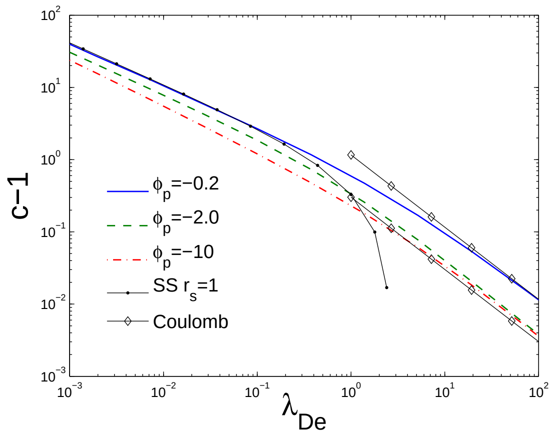

Figure 11: (Color online) Dimensionless probe capacitance in CE plasmas for $\tau = 1$ (a) and $\tau = 0.1$ (b) as a function of λ_{De}, for $\phi_p \geq -10$. "SS, $r_s = 1$" asymptotes correspond to the strong shielding solution (Eq. (72), and "Coulomb" asymptotes to Eq. (67).

a) $\tau = 1$

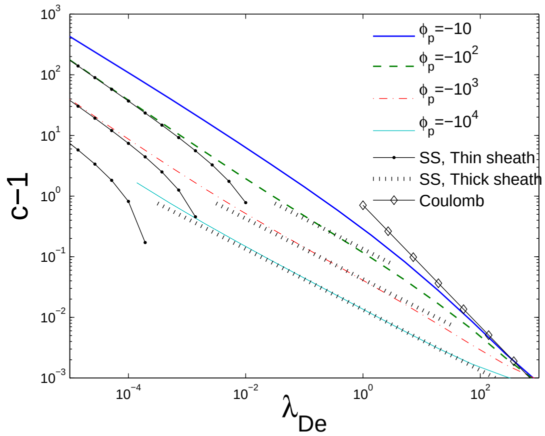

b) $\tau = 0.1$

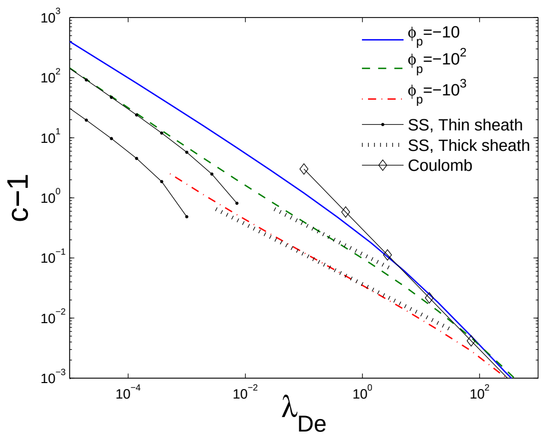

Figure 12: (Color online) Dimensionless probe capacitance in CE plasmas for $\tau = 1$ (a) and $\tau = 0.1$ (b) as a function of λ_{De}, for $\phi_p \leq -10$. "SS, Thin sheath" and "SS, Thick sheath" curves correspond to the strong shielding solutions respectively given by Eq. (74) and Eq. (75). "Coulomb" asymptotes correspond to Eq. (67).

the intuition that shortening the Debye length increases the shielding. Second c tends to 1 as $|\phi_p|$ increases, indicating that for strong biases the effective shielding length is much longer than λ_{De}.

10 Capacitance with Kinetic electrons

10.1 Analytic solutions

10.1.1 Coulomb limit

Applying the general form for the Coulomb limit capacitance given by Eq. (66) to KE plasmas (with $\Gamma_i^p/\tilde{\Gamma}_i^0$ given by Eq. (40)), we obtain

$$c^{\text{Coul}} = 1 + \frac{1}{\lambda_D}\left(1 + \frac{1}{(1+\tau)(\exp(\phi_p/\tau) - 1)}\right). \tag{76}$$

Contrary to its CE plasma counterpart (Eq. (67)), Eq. (76) allows the capacitance to be lower than 1 (when $\phi_p > \tau \ln\ (\tau/(1+\tau))$), and even negative when

$$\lambda_D < \frac{1}{(1+\tau)(1-\exp(\phi_p/\tau))} - 1. \tag{77}$$

Eq. (76) is only valid when $\lambda_{De} \gg 1$, therefore the prediction of Eq. (77) is only expected to be accurate for $|\phi_p|/\tau \ll 1$. The trend is however clear: the weaker the probe bias, the higher a Debye length is needed to ensure a positive capacitance. This is in agreement with the quasineutral analysis performed in Paragraph 3.2.

When $|\phi_p|/\tau \gg 1$, Eq. (76) reads

$$c^{\text{Coul}} = 1 + \frac{1}{\lambda_D}\frac{\tau}{1+\tau}, \tag{78}$$

in other words the strong bias Coulomb capacitance is the same as for CE plasmas (Eq. (69)).

10.1.2 Strong shielding

In the strong shielding limit ($\lambda_{De} \ll r_s$), two possibilities should be considered. If we are in the strong bias regime, the capacitance formulas for CE plasmas apply (Eq. (73) and Eq. (75)).

If we are in the weak bias regime, the capacitance is negative, and we can not calculate it as our continuum model breaks down.

10.2 Numerical solutions and physical discussion

Fig. (13) shows the probe dimensionless capacitance defined by Eq. (64) as a function of λ_{De} in KE plasmas.

It is convenient to analyze Fig. (13) from large to small Debye length. For $\lambda_{De} \gg \max(1, |\phi_p|/\min(1,\tau))$ Eq. (76) applies, as shown in Fig. (13a) in the case $\phi_p = -0.2$. For weak enough bias $c(\lambda_{De} = \infty) = 1^-$, and decreases down to negative values as λ_{De} is reduced.

For high enough biases ($\phi_p \lesssim -1$ in the equithermal case), $c(\lambda_{De} = \infty) = 1^+$ and increases up to a maximum with decreasing λ_{De}, before turning negative as $\phi_t \lesssim \phi_p$ (Eq. (28)). Of course for $\lambda_{De} \gg \max(1, |\phi_p|/\min(1,\tau))$ Eq. (76) would apply, but because we plot c rather than $c-1$ the agreement between theory and computation would hardly be visible on the figure.

As shown in Section 4, provided $\lambda_{De} \gtrsim 10^{-5}$ CE and KE results are indistinguishable (strong bias regime) when $|\phi_p| \gtrsim 10$. In other words, the curves labeled "$\phi_p = -10, -10^2, -10^3$" in Fig. (13) are virtually identical to those in Fig. (12). The strong bias analytic results derived in the previous section (Eq. (73) and Eq. (75)) are still valid here, although we have not plotted them in Fig. (13).

11 Summary and conclusions

In summary, we provided the first full numerical solution to the idealized problem of the interaction of a non-emitting spherical body with a continuum plasma, considering both fully collisional and collisionless electrons as outlined in Paragraph 2.1. Areas of investigation included collected fluxes (Sections 4,5,6), floating potentials (Sections 7,8) and capacitances (Sections 9,10).

By adopting the zero-density inner boundary condition, we were able to reduce the dimensionless

a) $\tau = 1$

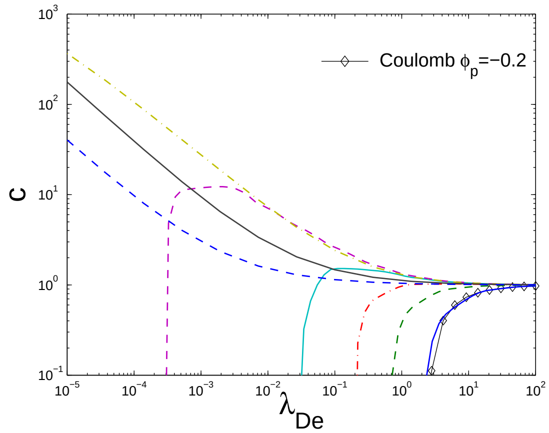

b) $\tau = 0.1$

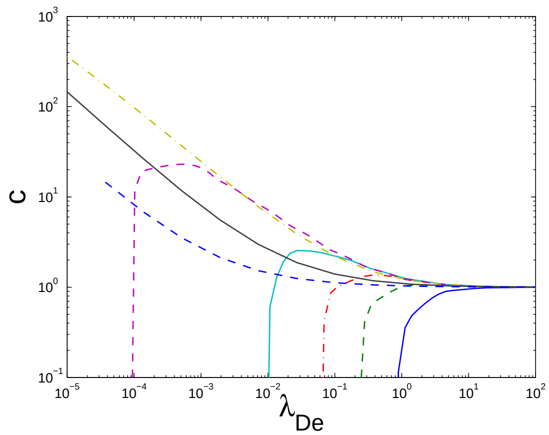

c) $\tau = 0.01$

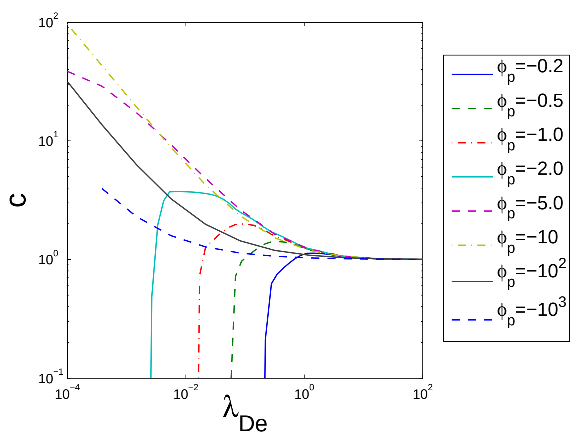

Figure 13: (Color online) Dimensionless probe capacitance in KE plasmas for $\tau = 1$ (a), $\tau = 0.1$ (b) and $\tau = 0.01$ (c) as a function of λ_{De}. "Coulomb $\phi_p = -0.2$" refers to Eq. (76) with $\phi_p = -0.2$.

parameter space to τ (ion to electron temperature ratio), ϕ_p (probe bias) and λ_{De} (electron Debye length); diffusivity ratios D_e/D_i or D_e^{app}/D_i replace ϕ_p as free parameter when we solve for the floating potential. We however showed that the key parameter governing the shielding is not λ_{De}, but the electron Debye length to sheath radius ratio λ_{De}/r_s.

Comparison with existing, or in most cases new analytic asymptotic solutions (referenced in Tab. 2), helps to understand the physics behind our computational results. In particular we showed that with the exception of the intermediate shielding regime defined in Tab. 1 ($r_s/10 \leq \lambda_{De} \leq 10r_s$), there aways exists a closest asymptotic regime whose analytic solutions are accurate to 15% or better.

This work concludes more than 40 years of research on an admittedly extremely idealized model of plasma-probe interaction, by resolving long-standing contradictions, establishing the validity of previous approaches, and proposing a rigorous classification of operational regimes that can possibly set the basis for the analysis of more elaborated models.

Acknowledgments

The authors would like to thank H. Noguchi and M. Tanaka at Keio University for hosting L. Patacchini during the development of the Finite Element code, as well as T. Tanahashi for very valuable discussions.

Leonardo Patacchini was supported in part by NSF/DOE Grant No. DE-FG02-06ER54891.

References

[1] I.H. Hutchinson, *Principles of Plasma Diagnostics*, 2nd ed. (Cambridge University press, Cambridge, UK, 2002).

[2] J.D. Swift and M.J.R. Schwar, *Electrical Probes for Plasma Diagnostics* (Iliffe Books, London, 1969).

[3] P.M. Chung, L. Talbot and K.J. Touryan, *Electric Probes in Stationary and Flowing Plasmas: Theory and Application* (Springer, New York, 1975).

[4] R.M. Clements and C.S. MacLatchy, J. Appl. Phys. **43**(1) 31-37 (1972).

[5] M. Kamitsuma and S.L. Chen, J. Appl. Phys. **48**(12) 5347-5348 (1977).

[6] V.E. Fortov, A.C. Ivlev, S.A. Khrapak, A.G. Khrapak, and G.E. Morfill, Phys. Reports **421** 1-103 (2005).

[7] A.F. Pal, A.V. Filippov and A.N. Starostin, Plasma Phys. Control. Fusion **47** B603-615 (2005).

[8] C.H. Su and S.H. Lam, Phys. Fluids **6**(10) 1479-1491 (1963).

[9] I.M. Cohen, Phys. Fluids, Phys. Fluids **6**(10) 1492-1499 (1963).

[10] E. Baum and R.L. Chapkis, AIAA Journal **8**(6) 1073-1077 (1970).

[11] R.J. Cicerone and S.A. Bowhill, *Positive ion collection by a spherical probe in a collision-dominated plasma* (Aeronomy report 21, University of Illinois Urbana, 1967).

[12] R.E. Kiel, J. Appl. Phys. **40**(9) 3668-3673 (1969).

[13] D.L. Thomas, Phys. Fluids **12**(2) 356-359 (1968).

[14] R.L. Chapkis and E. Baum, AIAA Journal **9**(10) 1963-1968 (1971).

[15] L.G. D'yachkov, A.G. Khrapak and S.A. Khrapak, J. Exp. Theor. Phys. **106**(1) 166-171 (2008).

[16] E.W. MacDaniel and E.A. Mason, *The mobility and diffusion of ions in gases* (Wiley, New York, 1973).

[17] I.H. Hutchinson and L. Patacchini, Phys. Plasmas **14**(1) 013505 (2007).

[18] S.A. Khrapak, S.K. Zhadanov, A.V. Ivlev and G.E. Morfill, J. Appl. Phys. **101**(3) 033307 (2007).

[19] S.A.Khrapak, G.E. Morfill, A.G Khrapak and L.G. D'Yachkov, Phys. Plasmas **13** 052114 (2006).

[20] J.S. Chang and J.G. Laframboise, Phys. Fluids **19**(1) 25-31 (1976).

[21] Y.L. Alpert, A.V. Gurevich and L.P. Pitaevskii *Space Physics with Artificial Satellites* (Consultants Bureau, New York 1965).

[22] I.B. Bernstein and I.N. Rabinowitz, Phys. Fluids **2**(2) 112-121 (1959)

[23] K.U. Riemann, J. Phys D: Appl. Phys **24** 493-518 (1991).

[24] A.D. Brailsford, J. Appl. Phys. **48**(4) 1753 -1755 (1977).

[25] I.H. Hutchinson, Plasma Phys. Control. Fusion **48**, 185-202 (2006).